Materials and Design 52 (2013) 47–57

Contents lists available at SciVerse ScienceDirect

Materials and Design

journal homepage: www.elsevier.com/locate/matdes

Dry sliding and tribocorrosion behaviour of hot pressed CoCrMo biomedical alloy as compared with the cast CoCrMo and Ti6Al4V alloys

Z. Doni [a,b], A.C. Alves [a], F. Toptan [a,*], J.R. Gomes [a,c], A. Ramalho [d], M. Buciumeanu [b], L. Palaghian [b], F.S. Silva [a,c]

[a] Centre for Mechanics and Materials Technologies (CT2M), Universidade do Minho, Azurém, 4800-058 Guimarães, Portugal
[b] Faculty of Mechanical Engineering, "Dunarea de Jos" University of Galati, Galati, Romania
[c] Universidade do Minho, Dept. Eng. Mecânica, Azurém, 4800-058 Guimarães, Portugal
[d] CEMUC – Department of Mechanical Engineering, University of Coimbra, 3030 Coimbra, Portugal

ARTICLE INFO

Article history:
Received 8 February 2013
Accepted 14 May 2013
Available online 23 May 2013

Keywords:
CoCrMo
Dry sliding
Hot pressing
Ti6Al4V
Tribocorrosion

ABSTRACT

Alternative processing routes are being widely studied for biomedical implant materials. Hot pressing (HP) is a powder metallurgy (P/M) process that combines the pressing and sintering steps simultaneously and therefore, provides a simpler production route with further advantages. However, dry sliding and tribocorrosion behaviour of HP CoCrMo alloy is yet to be studied. Since the implants are exposed to wear stresses and corrosive environments during their lifetime, tribocorrosion is an important issue for the implant materials. Thus, the present work aims at evaluating the dry sliding and tribocorrosion behaviour of the HP CoCrMo implant material as compared with the widely used commercial cast Ti6Al4V and CoCrMo implant materials. All tribological experiments were carried out under 1 N normal load, 1 Hz frequency and 3 mm total stroke length, using a reciprocating ball-on-plate tribometer. Tribocorrosion experiments were performed at both room and the body temperatures, in 8 g/l NaCl solution. Open circuit potential (OCP) was measured before, during and after sliding. Worn surfaces investigated by field emission gun scanning electron microscope (FEG-SEM) equipped with energy dispersive X-ray spectroscopy (EDS), and the wear rates were calculated using a profilometer. Results suggest that all PHCoCrMo samples presented better wear resistance after both dry sliding and tribocorrosion tests. Additionally, as compared to the cast CoCrMo samples, HP CoCrMo samples presented better wear resistance in dry sliding conditions and similar wear resistance in tribocorrosion conditions. Due to the experimental results, it may be suggested that HP can be considered as a simple and low cost alternative production route for CoCrMo implant materials.

1. Introduction

Titanium and its alloys are widely used in orthopaedic and dental implants due to their mechanical properties, high corrosion resistance, and adequate biocompatibility. However, a major problem of Ti and its alloys is their low wear resistance, which raises major clinical concerns [1–3]. CoCrMo alloys on the other hand, exhibit the most useful balance in strength and wear resistance among all implant materials, together with the corrosion resistance [4,5], thus CoCrMo alloys are suitable for self-bearing applications, having either low or high carbon contents [6].

When an implant material attached to the bone, during the cyclic loads, relative movements cause wear stresses due to the difference of Young's Modulus between the bone and the implant. Therefore, wear resistance is crucial for implant materials [3,7]. On the other hand, corrosion damage is also a very important issue for metallic implants that can affect the biocompatibility and mechanical integrity [8]. It has been reported that 20–30% material loss can be attributed to corrosion-related damage, not only includes the pure corrosion process but also the wear induced/enhanced corrosion process that is defined as tribocorrosion [9]. Tribocorrosion is an irreversible process that occurs on the surface causing a deterioration of the material due to the combined wear and corrosion actions that simultaneously take place during the sliding [10]. Another consequence of the tribocorrosion action is the metal ion releasing, that is still one of the major concerns related to the clinical aspects and the lifetime of the metallic implant materials [11].

Molinari et al. studied the dry sliding wear mechanism of the Ti6Al4V alloy, sliding against the alloy itself at different loads and sliding speeds. The authors reported oxidative and delamination wear, and emphasized the low resistance of the alloy to plastic deformation even at low loads as well as the poor protection of the

* Corresponding author. Tel.: +351 253 510220; fax: +351 253 516007.
E-mail address: ftoptan@dem.uminho.pt (F. Toptan).

0261-3069/$ - see front matter © 2013 Elsevier Ltd. All rights reserved.
http://dx.doi.org/10.1016/j.matdes.2013.05.032

surface oxide layer [1]. Another study by Borgioli et al. used as well Ti6Al4V against itself and it was reported oxidation and delamination wear, as well as a transition from oxidation to delamination at lower sliding speeds [12].

The effect of the oxide layer on the dry sliding wear behaviour of the Ti6Al4V alloy has been studied by Ming et al. The authors performed tests against GCr15 steel using a high speed pin-on-disc tribometer and reported the formation of the oxides of TiO, TiO_2, and V_2O_3 as the frictional temperature increases. It has also been stated that the wear resistance of the alloy rapidly decreased due to the loosen oxide layer [13]. Alam and Haseeb studied the dry sliding wear behaviour of Ti6Al4V alloy against hardened-steel, under various loads and a constant unidirectional sliding speed. The authors reported deep grooves, gross plastic deformation, severe delamination and severe adhesion on the worn surfaces of the Ti6Al4V alloy [14].

Saldívar-García and López studied the dry sliding wear behaviour of cast and wrought CoCrMo alloys sliding against the alloy itself, using a pin-on-disc tribometer. The authors stated that microstructural features played an important role on the wear behaviour of the alloy. Plastic deformation and the oxidized wear debris after wear tests have also been reported by the authors [15]. The wear properties of high nitrogen CoCrMo alloys against the alloy itself have been studied by Hsu and Lian, and it has been concluded that the main effect on the wear resistance of the CoCrMo alloys are grains size and HCP/FCC ratio [16].

The tribocorrosion phenomenon is still being studied by several researchers in order to understand the degradation mechanism during the lifetime of the implant materials. Barril et al. studied the effect of electrochemical conditions on the tribocorrosion behaviour of the Ti6Al4V alloy against alumina. The authors concluded that wear is deeply affected by applied potential affecting the characteristics of the passive film. The authors also investigated the effect of the amplitude and the normal load on the tribocorrosion behaviour of Ti6Al4V/alumina pair in 0.9% NaCl solution. It has been reported that wear accelerated corrosion occurs in Ti6Al4V/alumina contacts, only if the sliding amplitude is large enough to induce slip between the two mating surfaces [17]. The tribocorrosion behaviour of Ti6Al4V alloy against 316 stainless steel in artificial seawater has been studied by Jun and Feng-yuan. The authors indicated that the synergism action between corrosion and wear was related to the corrosion rate, furthermore, with the increase of corrosion rate, the synergism became more important [18]. On the other hand, Martin et al. studied the tribocorrosion behaviour of Ti6Al4V alloy against alumina ball in 1% NaCl solution and reported that the hardness was the controlling factor for the tribocorrosion behaviour. Furthermore, the corrosion resistance was found to be depended on the microstructure and the texture of the surface [19]. Dimah et al. studied the tribocorrosion behaviour of wrought titanium alloys (Ti-Grade 2, Ti6Al4V, and Ti6Al4V-ELI) against an alumina ball in phosphate buffered solution with and without the presence of proteins. The authors reported that the alloying elements of Ti6Al4V reduced the active and passive dissolution of the titanium and considerably decreased the wear accelerated corrosion under tribocorrosion conditions. Furthermore, the wear resistance of the Ti6Al4V alloy with $\alpha + \beta$ phase microstructure is reported as substantially higher than that of the Ti Grade 2 α phase microstructure under the studied conditions [20].

Muñoz and Julián studied the tribocorrosion behaviour of a high carbon CoCrMo alloy sliding against alumina in simulated body fluids, and reported that the wear of CoCrMo alloy was negligible under cathodic and in the cathodic–anodic transition and considerably increased in the passive domain. The formation and removal of the passive films during sliding is reported to lead to a progressive material loss. The authors also stated that the three-body effect depended on surface chemistry, which also varied due to the solution chemistry and applied potential, and therefore modified the tribocorrosion rate [21]. Mathew et al. investigated the tribocorrosion behaviour of low-carbon CoCrMo alloy against alumina ball in phosphate buffer solution and bovine calf serum. The authors reported that except for the highest load which corresponds to 752 MPa initial Hertzian contact pressure, the dominant material loss mechanism was wear–corrosion, however, mechanical wear was dominant at the highest load [22]. Yan et al. studied the tribocorrosion behaviour of high carbon CoCrMo and low carbon CoCrMo alloys against a silicon nitride ball in three different biological solutions including 0.36% NaCl solution at 37 °C and stated that corrosion plays an important role in the total degradation process [23].

Although production of implant materials by conventional methods -as investment casting technique which is widely used for CoCrMo implant materials- are common, powder metallurgy (P/M) route offers further advantages namely eliminating casting defects such as uncontrolled porosity, chemical inhomogeneity, large grain size and microstructure with hard precipitates in the interdendritic zones. It has been shown that the properties of P/M implants are comparable with those of the wrought alloys [4,24]. HP is a P/M process where loose powder is loaded into a mould, usually of graphite, and sintered by the simultaneous application of high temperature and pressure [25]. HP technique is known for producing better mechanical and electrochemical properties as compared to the conventional techniques, as well as providing a simpler fabrication process [26–28]. However, dry sliding and tribocorrosion behaviour of HP CoCrMo alloy is yet to be studied. Thus, the aim of this study was to investigate the dry sliding and tribocorrosion behaviour of the HP CoCrMo implant material as compared with the widely used commercial cast Ti6Al4V and CoCrMo implant materials.

2. Experimental procedure

2.1. Materials

HP CoCrMo samples were produced using spherical CoCrMo powders (Nobil 4000, Nobilmetal, Villafranca d'Asti, Italy) having a mean particle size ranged between 20 and 40 μm. Cast commercial CoCrMo (Nobil-Metal Alloys & Solders Company, Italy) and Ti6Al4V alloys (Bunting Titanium, UK) were used for the comparison. The chemical compositions of the powder and the commercial alloys are given in Tables 1 and 2.

2.2. Processing

Prior to the processing, CoCrMo powders were dried in a muffle furnace at 105 °C, for 1 h in order to remove the humidity. For the HP procedure, CoCrMo powders were inserted into a graphite die having 10 mm diameter. In order to avoid the contamination, die walls were painted with zirconia paste. The graphite die was mounted in to a hydraulic press and heated up to 1000 °C with a heating rate of 18 °C/min, using an induction furnace (Easyheat 5060 CE Ameritherm). The entire process was performed under vacuum (0.01 mbar), and at a constant pressure (40 MPa) with a sintering time of 30 min. The temperature was monitored during the whole process, using a Type K thermocouple connected to a data logger (National Instruments – NI SCXI-1000). The schematic representation of the HP process is given in Fig. 1.

Prior to the each test, the samples were ground down to 4000 mesh size SiC paper followed by polishing with diamond paste down to 1 μm. After polishing, samples were ultrasonically cleaned in propanol for 10 min followed by distilled water during 5 min.

Table 1
Chemical compositions of the cast CoCrMo alloy and CoCrMo powders according the manufacturers (wt%).

Material	Co	Cr	Mo	Si	Fe	Mn	W	Ni	C
Alloy	Balance	31.0	4.0	2.2	Trace	Trace	Trace	–	–
Powder	Balance	28.0–30.0	5.0–6.0	Trace	–	Trace	–	Trace	Trace

Table 2
Chemical compositions of the cast Ti6Al4V alloy according the manufacturer (wt%).

Elements	Al	V	Fe	Sn	Ni
Ti–6Al–4V	6.1	4.21	0.2	0.003	0.01

The samples were kept in a desiccator for 24 h before starting the tests, in order to obtain the similar surface conditions. Vickers hardness was calculated as a mean of 5 indentations per sample using a Shimadzu microhardness tester at a load of 500 g during 15 s.

2.3. Dry sliding wear tests

Dry sliding tests were performed on a tribometer (CETR-UMT-2) using ball-on-plate configuration and reciprocating plate adapter generating a harmonic wave. An alumina ball of 10 mm diameter (Goodfellow) was used as a static counter material and the samples were the moving body. The tests were performed in ambient air (24 ± 2 °C), under 1 N normal load, at a frequency of 1 Hz, and the total stroke length of 3 mm during 1800 s.

2.4. Corrosion tests

Open circuit potential (OCP) and potentiodynamic polarization measurements were carried out in 8 g/l of NaCl solution at both room (24 ± 2 °C) and body (37 ± 2 °C) temperatures, using Gamry Potentiostat/Galvanostat (model Reference-600). Prior to the tests, the pH values of the electrolyte were measured on pH-meter (EUTECH Instruments pH 510) as 5.74 ± 0.04 and 5.72 ± 0.04 for room and body temperatures, respectively. A standard three-electrode electrochemical cell (adapted from *ASTM: G3-89*) with an electrolyte volume of 200 ml was used for the electrochemical measurements, where saturated calomel electrode (SCE) used as the reference electrode, Pt electrode used as the counter electrode, and samples having an exposed area of 0.38 cm^2 used as the working electrode. Potentiodynamic polarizations were performed by using an initial delay time at equilibrium state of 60 min in order to stabilize the surface at OCP. A polarization scan was carried out in the anodic direction up to 1 V/SCE, starting at 0.25 V/SCE more negative than (E_{OCP}), at a rate of 1 mV/s.

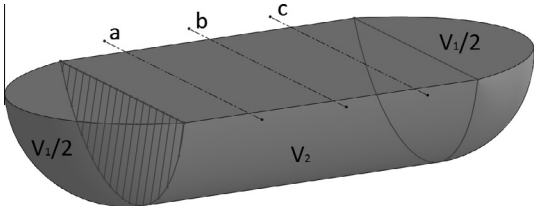

Fig. 2. The estimated model used for calculating the wear loss volume. The lines a, b, and c are indicating the 2D profile lines.

2.5. Tribocorrosion tests

For the tribocorrosion tests, the electrochemical cell was installed on a ball-on-plate tribometer (CETR-UMT-2) with the working surface are of the samples facing upwards, against the counter material (10 mm diameter alumina ball, Goodfellow). The electrochemical measurements were carried out at both room and body temperatures using the same three-electrode set-up, together with the same equipment and 30 ml of the same electrolyte (8 g/l of NaCl) that used in corrosion tests. Since the work aims at comparing tribocorrosion behaviour of three different samples, measurement of corrosion potential is chosen as a triboelectrochemical technique owing to its simplicity for gathering information on the surface state of the sliding metals [29]. Thus, OCP was measured before, during and after sliding where the sliding action started after reaching the stable OCP values for each test. The tribological parameters were chosen the same as the dry sliding tests (1 Hz, 3 mm, 1 N, and 1800 s).

2.6. Wear rate

The volume loss values were determined by following the wear track model represented in Fig. 2. The length of the wear track was taken as 3 mm (i.e. the total stroke length) and the tips of the wear track were assumed as a part of a calotte. The width and the deepness of the wear track were measured by a contact profilometer (Mitutoyo Surftest SJ-500). For each wear track, three 2D profiles were obtained from the centre of the wear track (line b in Fig. 2), and 1 mm away from the centre for both sides (lines a and c in

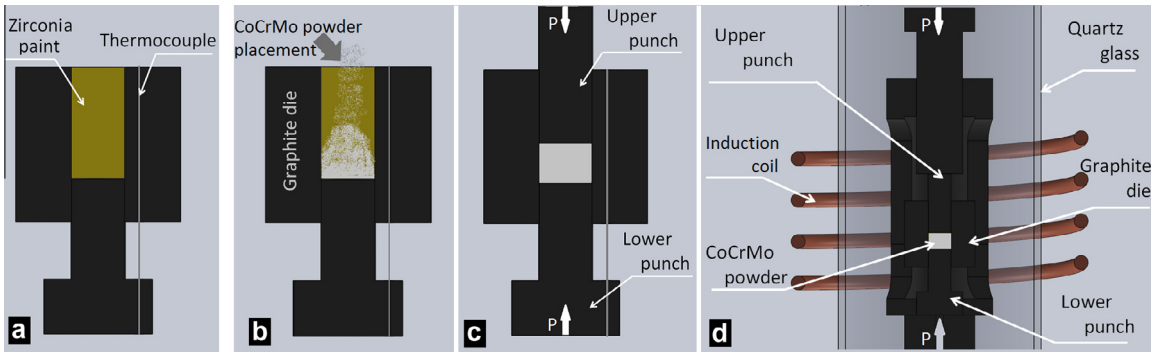

Fig. 1. Schematic representation of the HP process: (a) painting of the die walls by zirconia, (b) introducing the alloy powder, (c) applying the pressure, and (d) overall representation of the system.

Fig. 2). For the calculation of wear loss volume, first, wear loss area for each 2D profile was calculated with the following formula:

$$A_w = \sum_{i=0}^{n} 0.5(Y_i + Y_{i-1})(X_i - X_{i-1}) \quad (1)$$

where A_w is the wear loss area for each 2D profile in mm^2, X is the width in mm, Y is the deepness in mm, and n is the number of counts. Then, average deepness values were calculated with the following formula:

$$\overline{D} = \frac{\overline{A}_w}{\overline{W}} \quad (2)$$

where $\overline{D}$ is the average depth in mm, $\overline{A}_w$ is the average wear loss area of three 2D profiles for each wear track, and $\overline{W}$ is the average width of each wear tracks measured for three 2D profiles. Finally, wear volume was calculated with the following formula:

$$\Delta V = \left[\frac{1}{3} * \pi * \overline{D}^2(3R - \overline{D})\right] + \overline{A}_w * l \quad (3)$$

where ΔV is the total volume loss for each wear track in mm^3, R is the radius of the alumina ball, and l is the total stroke length which was constant for all tests as 3 mm. The volume loss values were converted into wear rate with the following formula:

$$W_v = \frac{\Delta V}{S} \quad (4)$$

where W_v is the wear rate in mm^3/mm, ΔV is the volume loss of the sample in mm^3, and S is total sliding distance in mm.

All tests were repeated at least three times in order to have repeatability in terms of COF. Wear rates were calculated from three tracks per condition.

2.7. Microstructural characterization

After the dry sliding and the tribocorrosion tests, samples were ultrasonically cleaned in propanol for 10 min followed by distilled water for 5 min and worn surfaces were characterized using FEI Nova 200 Field Emission Gun scanning electron microscope (FEG-SEM) equipped with EDAX, energy dispersive X-ray spectroscopy (EDS).

3. Results and discussion

3.1. Dry sliding wear behaviour

Zivic et al. studied the dry sliding wear behaviour of Ti6Al4V alloy against alumina, under a range of loads varying between 0.1 and 1 N, and sliding speeds varying between 4 and 12 mm/s under reciprocating sliding mode. The authors reported that the Ti–Al intermetallic compounds that may be occurred during the sliding could contribute to the abrasive wear due to their higher hardness values. The authors also stated that abrasive wear was the dominant wear mechanism up to 10 m sliding distance under 0.5 N normal load, which corresponds to 1158.73 MPa initial Hertzian contact pressure [30]. In the present work, the sliding distance (10.8 m) and the average sliding speed (6 mm/s) was similar to the ones that applied by Zivic et al. However, the initial Hertzian contact pressure was relatively lower (412.15 MPa). Even though, it is possible from the microstructural investigations to state that abrasive wear was the dominant wear mechanism that is represented by parallel grooves (Fig. 3a). However, grooves were not the only feature that was observed on the worn Ti6Al4V surfaces. It is found from the microstructural studies and EDS analysis that due to the repetitive material transfer from the sample to the counter material during the sliding, adhered/mixed patches were formed on the worn Ti6Al4V surfaces. However, the effect of wear debris clusters on the wear mechanism is rather clear. It has been reported that Ti–Al intermetallic compounds (Ti_2Al_3, Al_3Ti) may occur during the sliding of Ti alloy against alumina and those intermetallic particles may cause three-body abrasion that may significantly increase the wear rate. On the other hand, titanium oxides (e.g. TiO_2) may also be formed on the wear surface during the sliding and may lower the coefficient of friction [30,31]. In the present study, once that the wear debris generated were not enough for XRD studies, a detailed chemical characterization studies could not be performed on the wear debris, in order to understand if they are mainly composed of intermetallic particles or titanium oxides. However, when the EDS analysis of the patches and "clean" wear track areas are compared, it was observed that Al and O content is higher on the patch areas. Since those patches were assumed as an adhered/mixed material, it can be expected that the patches may also have the composition of the wear debris. Similarly, it has been previously reported that the loose wear debris has the same structure and composition as the transferred layer [32,33]. Thus, it is considered that the wear debris may contain the mixture of intermetallic compounds, fragments of counter material, and titanium oxides.

In further examinations, micro cracks were also detected on the worn Ti6Al4V surfaces (Fig. 3b). Delamination wear that occurs due to the nucleation, growth and the connection of the cracks by the cyclic loads have been reported for the Ti6Al4V alloys by several authors [2,3,14,34,35]. However, from the worn surface investigation, it is not so easy to conclude a delamination wear for the worn Ti6Al4V after dry sliding wear tests. Considering the BSE SEM image on the Fig 3b together with the EDS analysis, it has been deduced that the cracks were mainly occurred on the adhered layers.

Straffelini and Molinari studied dry sliding wear behaviour of Ti6Al4V alloy sliding against both the alloy itself and AISI M2 steel under different sliding speeds and loads. The authors reported that a noticeable surface plastic deformation and a subsurface strain-hardening region of about 40 μm in depth were found in all samples and all testing parameters. The authors also pointed the strain-hardening phenomena that occurred during the sliding [35]. Fig. 3c represents the BSE SEM image of the alumina ball slide against Ti6Al4V sample. As can be seen on the image, an important amount of the alloy was transferred to the ball during the sliding, which indicates the adhesive wear. The hardness of the transferred alloy may be increased dramatically due to the strain hardening effect, as well as the intermixing of the oxide fragments [35]. Therefore, due to the high hardness, this hardened layer may be cracked easily compared to the base alloy. Thus, this mechanism may also contribute to the formation of the microcracks on the worn surfaces. However, subsurface structure of the worn area should also investigated in order to characterize the delamination wear. So far, due to the subsurface cracks, delamination wear may also have occurred in some regions and those delaminated regions may be covered by the adhered material. However, since the wear tracks were too small, clear characterization of the subsurface area could not be performed.

Therefore, after microstructural investigations and elemental analysis, the dry sliding wear mechanism for the Ti6Al4V alloy may be suggested as mainly the combination of abrasive and adhesive wear.

The worn surfaces of the CoCrMo samples presented similar structures both for cast and hot pressed samples. Deep and well aligned grooves were presented in all tracks (Fig. 4a). Mu et al. studied the dry sliding wear behaviour of CoCrMo against GGr15 steel. Even the contact pressure was reasonably lower (0.65 MPa) the authors reported that the worn surface of CoCrMo alloy was easily scratched during the sliding [36]. Indeed, abrasion is

commonly observed in metal-on-metal and other hip joint bearings as one of the most important biomedical application of the CoCrMo alloys [37]. It has been reported that abrasion may be induced by fractured carbides, compacted wear debris, and plastically deformed parts of the metal, or even contaminants from outside of the system [37]. On the other hand, during a sliding motion, chemical bonds between the surface atoms of two mating material may cause adhesive forces. It has been reported that the adhesion between the surface atoms of the mating materials is controlled by thermochemistry, and the degree of adhesion can be estimated by their mutual solubility [38]. It is known due to the Al–Co phase diagram that Co has a big amount of solubility in Al [39]. Therefore, during the sliding of CoCrMo alloy against alumina, adhesive wear can also be expected. Fig. 4a represents the adhesive wear features on the HP CoCrMo sample. Effect of the adhesive wear can also be visible on the surfaces of the counter material (Fig. 4b). An important amount of CoCrMo alloy was observed on the alumina ball surfaces in all testing conditions.

On the other hand, it was observed that in both samples, wear debris were accumulated and compacted on the preferential regions of the grooves, mainly on the wider grooves (Fig 4a). It has been reported that CoO, $CoCr_2O_4$, and Co_3O_4 are the main oxide compounds that are likely to occur during the sliding wear of the cast CoCrMo alloy [40]. EDS analysis taken from the accumulated wear debris zones presented relatively higher oxygen and aluminium peaks, as compared to the unworn surfaces. Thus, it may be suggested that the wear debris are mainly the mixture of oxides and fragments of the counter material.

Therefore, after microstructural investigations and elemental analysis, the dry sliding wear mechanism for the both cast and HP CoCrMo alloy may be suggested as a combination of abrasive and adhesive wear.

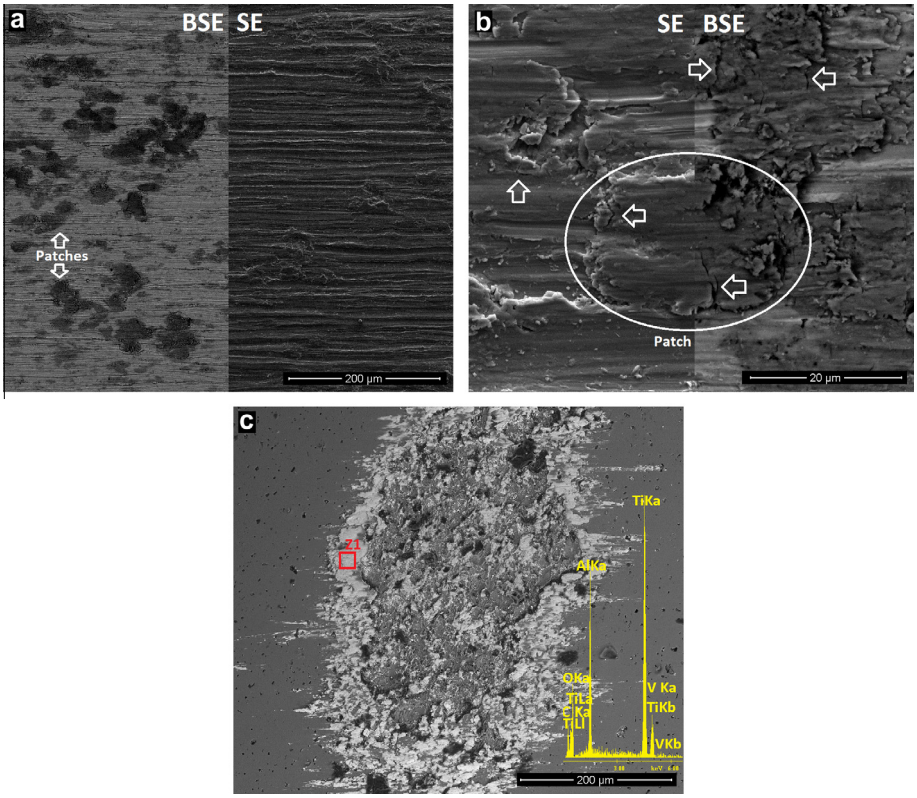

Fig. 3. (a) BSE/SE SEM image of the wear track of the Ti6Al4V sample, (b) detailed SE/BSE SEM image of the worn area (arrows indicates the micro cracks), and (c) BSE SEM image of the mating counter material surface, and the EDS spectra taken from the marked area (Z1).

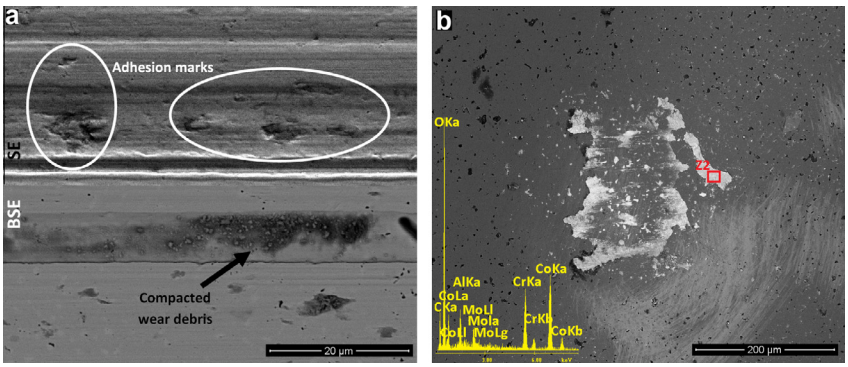

Fig. 4. (a) BSE/SE SEM image of the wear track of the HP CoCrMo sample and (b) BSE SEM image of the mating counter material surface, and the EDS spectra taken from the marked area (Z2).

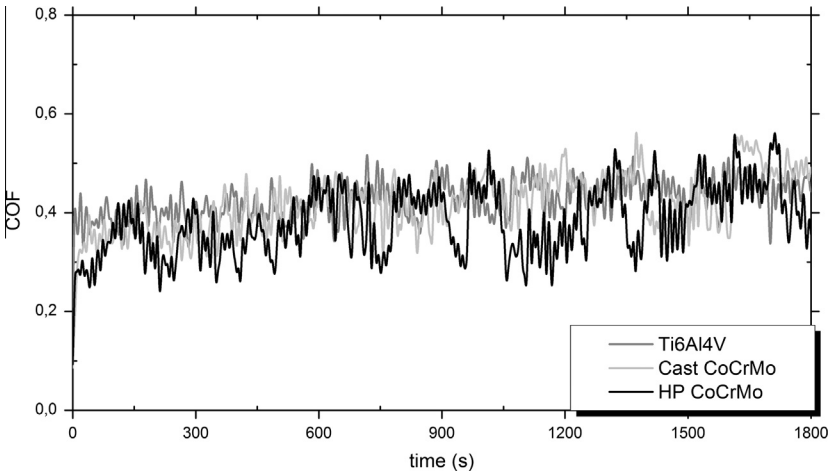

Fig. 5. Evolution of the coefficient of friction during dry sliding.

The evolution of the coefficient of friction (COF) during the dry sliding tests is presented in Fig. 5 for each sample. All samples presented average COF values of approx. 0.42 during the sliding. However, while the oscillations were relatively smaller during the first approx. 2 min of sliding, after that the oscillations increased.

Qu et al. studied the dry sliding wear behaviour of Ti6Al4V alloy against alumina. Even though the testing parameters were different than the present study, the authors presented similar evolution of COF having values in the range of 0.44–0.49, with relatively large oscillations. Since titanium alloy commonly transfers to the counter material during sliding against other ceramics, the authors explained the large oscillations of COF values by the formation and periodic localized fracture of a transferred layer [34]. On the other hand, three-body effect can also contribute to the oscillations on the COF values. As it stated before, the formation of intermetallics or the broken fragments of the counter material (alumina ball) may also be attributed to the three-body abrasion. Thus, the increased oscillations after approx. 2 min of sliding can be explained by the third body particles that formed by the fragmentation of the patches (Ti6Al4V) and the wear debris clusters (CoCrMo) on the worn surfaces (Figs. 3a, 3b, and 4a).

3.2. Corrosion behaviour

Polarization curves of the samples are given in Fig. 6 for both room and body temperatures, together with the average corrosion potential ($E_{(i=0)}$) and the average passivation current density (i_{pass}) values. Within the all groups of samples, similar polarization behaviour was observed for both temperatures. However, Ti6Al4V samples presented lower $E_{(i=0)}$ but higher i_{pass} and wider passivation range, as compared to the CoCrMo samples. On the other hand, no significant difference were observed between the cast and HP CoCrMo samples for both temperatures.

Pitting is known as one of the most common corrosion type for Co-based biomaterials [41]. However, even though an increase on the current density was observed after passivation plateau, no evidence of pitting corrosion was found neither from the polarization curves nor from the microstructural investigations of the CoCrMo samples within the testing conditions. Similar polarization curve was also observed by Henriques et al. under similar testing conditions [26]. On the other hand, Bettini et al. studied the corrosion behaviour of biomedical CoCrMo alloy in phosphate-buffered saline (PBS) solution and reported that the commonly observed current increase in the high anodic potential was not due to pitting corrosion, but due to a contribution of different reactions, including metal dissolution and electrochemical oxidation of water [42].

3.3. Tribocorrosion behaviour

The evolution of the COF during the sliding in NaCl solution is given in Fig. 7. COF values presented similar evolution both for room and the body temperature for all materials. However, while both cast and HP CoCrMo samples presented a relatively stable COF evolution, COF of Ti6Al4V slightly decreased during the sliding.

The evolution of OCP before, during and after sliding is also given in Fig. 7. Before sliding, the OCP values were stable for both temperatures in all samples due to the presence of a passive film on the alloy surfaces in contact with the electrolyte [43]. When sliding started, a sudden decrease occurred on the OCP values due to the damaging of the passive film by the mechanical action [44]. During the sliding, while both CoCrMo samples presented very similar and relatively stable OCP values, Ti6Al4V samples presented lower values together with a slight increment. Thus, it is possible to state that under tribocorrosion, CoCrMo samples presented lower tendency to corrosion within the testing conditions. However, it is worthy to remind that measurement of corrosion potential gives an information about the thermodynamic tendency to corrosion. Therefore, in order to understand the corrosion kinetics under sliding, potentiostatic and potentiodynamic tribocorrosion tests should also be performed [29,45].

After sliding, OCP values increased up to near the initial values recorded before the mechanical action due to the recovering of the passive film [29]. Repassivation of the metal surfaces after mechanical action is another important issue on tribocorrosion [46]. Contu et al. and Hanawa et al. reported that after a mechanical action, the repassivation rate can be determined by calculating the tangential rate at the initial repassivation curve [47,48]. The authors stated that the potential variation (ΔE) with the time followed a logarithm function of the time (t) as given below:

$$\Delta E = k_1 \log t + k_2 \quad (5)$$

Thus, k_1 represents the rate of repassivation within a certain range of time. In order to compare the repassivation behaviour of the samples, k_1 values were calculated for the period of 300 s after sliding by following the geometric model that represented in Eq. (5). As can be seen on the results (Fig. 8) Ti6Al4V samples presented slightly higher k_1 values as compared to CoCrMo samples.

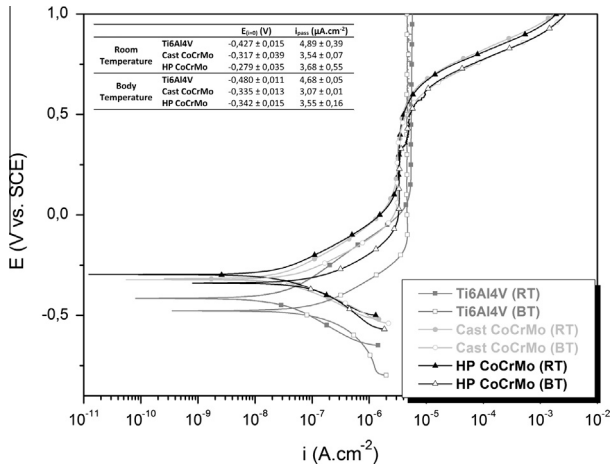

Fig. 6. Potentiodynamic polarization curves of the samples for both temperatures.

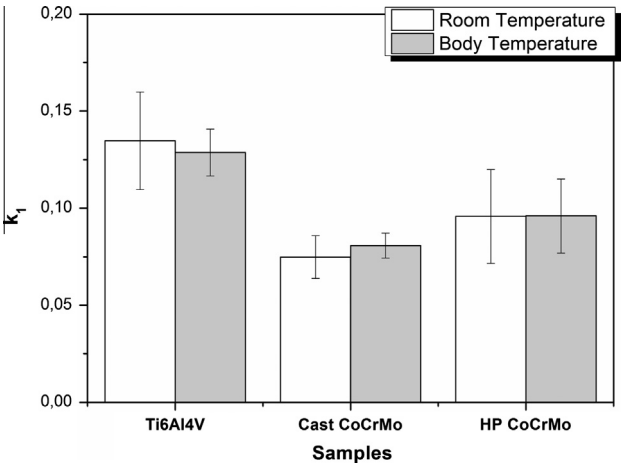

Fig. 8. Values of k_1 constants calculated by Eq. (5).

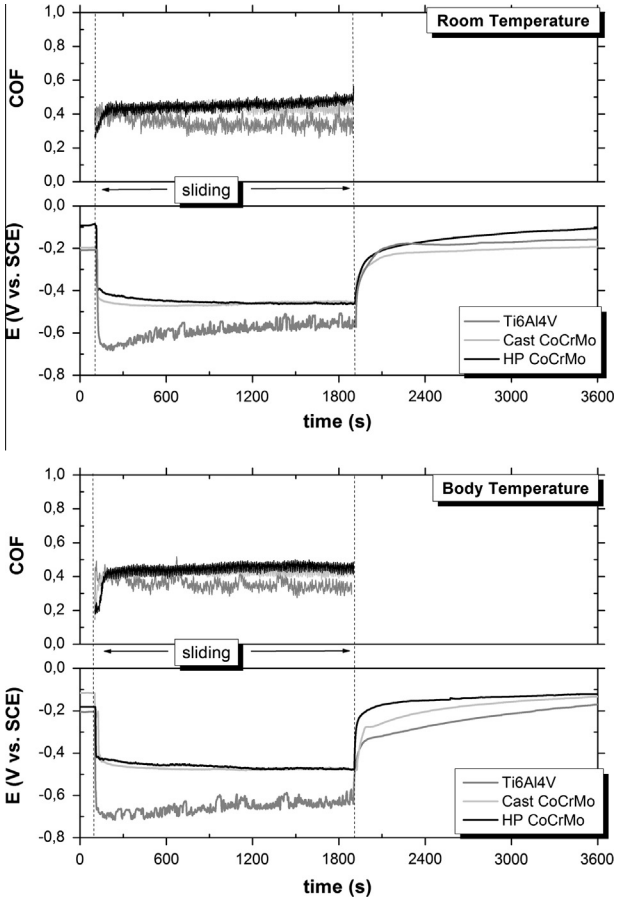

Fig. 7. Evolution of COF and OCP in NaCl solution (a) at room temperature, and (b) at the body temperature.

Hence, it can be suggested that the repassivation of Ti6Al4V was slightly faster than both CoCrMo samples. Furthermore, it is also possible to state that there were no significant influence of the temperature on the repassivation behaviour for all tested samples within the testing conditions and time range.

From the microstructural investigations, similar to the worn surfaces after dry sliding, adhered/mixed patches were observed on the worn Ti6Al4V surfaces after tribocorrosion tests (Fig. 9a). It was detected by EDS studies that those patches have relatively higher oxygen content. It is known that oxidation of titanium surface lowers the COF values [31]. Thus, slightly decreased COF values during the sliding of Ti6Al4V sample can be attributed to the formation of the patches. On the other hand, as compared to the worn surfaces after dry sliding tests, those patched were relatively smaller and more well distributed to the worn surface. Manhabosco et al. studied the tribocorrosion behaviour of Ti6Al4V against alumina ball in simulated body fluid solution. Especially after a run-in period, the authors observed relatively larger oscillations on the COF curve. The authors reported that the oscillations had been occurred due to the third body particles which had been entrapped between the sliding couple [49]. It has been reported that third body particles affects the tribocorrosion behaviour importantly. Landolt et al. stated that corrosion can accelerate or slow down the rate of mechanical material loss, depending on the properties of the third body particles [10]. The fragments that were loosely attached to the patches (Fig. 9a) may detach during the sliding and cause a third body effect. This also explains the relatively larger oscillations of the COF curve of the Ti6Al4V samples (Fig. 7). On the other hand, from electrochemical point of view, those well distributed patches lead to a more protective surface during the sliding. Therefore, OCP values were slightly increased during the sliding (i.e. tendency of corrosion decreased) for Ti6Al4V alloy (Fig. 7).

Fig. 9b shows a detailed view of the worn surfaces of Ti6Al4V samples after tribocorrosion tests in body temperature. Microcracks and material pull-out can be clearly seen on the surface. However, it is hard to conclude those features as delamination wear. Similar to the surfaces after dry sliding tests, those microcracks may be occurred on the transferred/hardened layer and pull-outs may be occurred due to the cold welding mechanism with the counter material. Once that the sliding was in a solution, those craters may not be filled by a transferred material as easy as dry sliding surfaces and that situation might make it possible to observe the craters easier after the tribocorrosion tests. On the other hand, similar to the ones after dry sliding, important amount of transferred alloy were found on the mating alumina ball surface (Fig. 9c). Therefore, the wear mechanism after tribocorrosion tests was also considered as a combination of abrasive and adhesive wear for Ti6Al4V alloy.

Fig. 10a represents the worn surfaces of HP CoCrMo sample after tribocorrosion tests. When compared to the worn surfaces after dry sliding tests, similar surface features were observed after tribocorrosion tests, except for the accumulated wear debris. This is probably due to the removing of wear debris in the solution during the testing. As a consequence of this behaviour, relatively smaller oscillations were observed on the COF curves during the

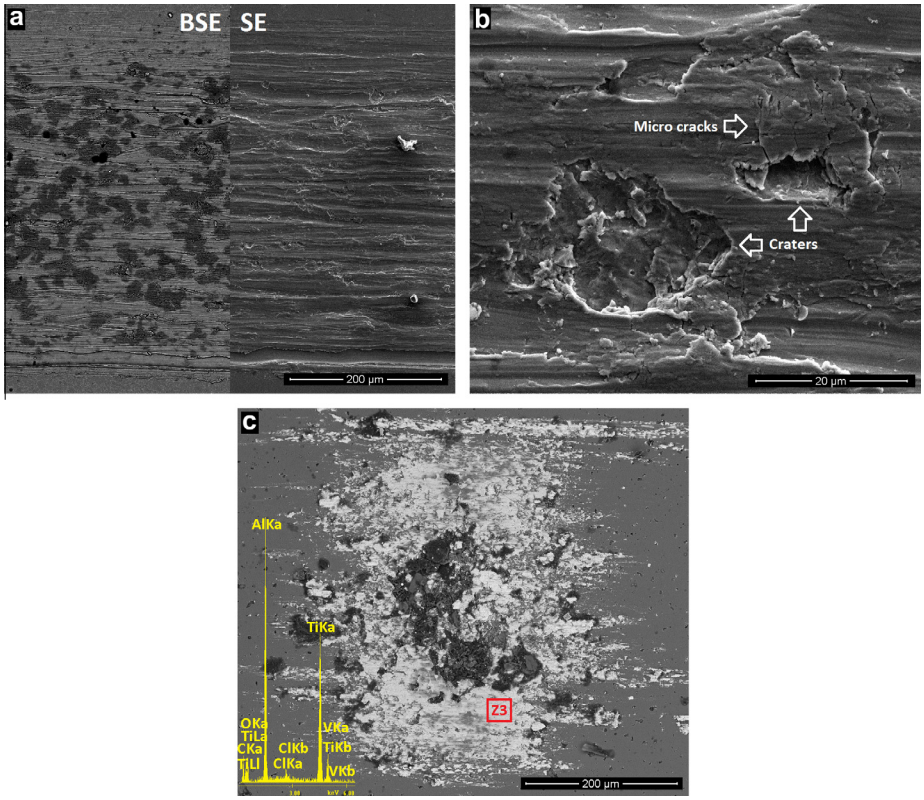

Fig. 9. Worn surfaces of samples after tribocorrosion tests; (a) BSE/SE SEM image of the wear track on the Ti6Al4V sample, (b) detailed BSE image of the marked area shows micro cracks and material pull-out (craters) on Ti6Al4V sample, and (c) BSE SEM image of the mating counter material surface, and the EDS spectra taken from the marked area (Z3).

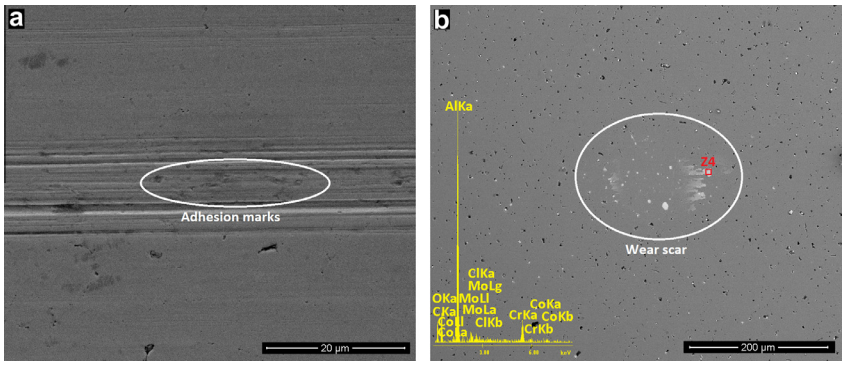

Fig. 10. (a) SE SEM image of the wear track on HP CoCrMo sample after tribocorrosion, and (b) BSE SEM image of the mating counter material surface, and the EDS spectra taken from the marked area (Z4).

sliding, due to the reduced third body effect. Furthermore, the OCP curves also presented more stable and smooth evolution during the sliding. This behaviour is also affected from the absence of the accumulated wear debris on the surface. Similar behaviour was observed also for the cast CoCrMo sample. On the other hand, adhesion marks were observed on the worn surfaces and even though it was a smaller amount as compared to the dry sliding case, transferred material was detected on the mating counter material surface (Fig. 10b). Therefore, it can be suggested that the wear mechanism was mainly as a combination of abrasive and adhesive wear for CoCrMo alloys after tribocorrosion tests.

3.4. Wear rate

The wear rate values after dry sliding and tribocorrosion tests are presented in Fig. 11. It is well known that CoCrMo alloys have higher wear resistance as compared to the Ti6Al4V alloys [5,50–52]. Thus, as can be expected, after dry sliding tests, the wear rate of Ti6Al4V alloy ($5.19 \times 10^{-7} \pm 8 \times 10^{-8}$ mm^3/mm) was 14 and 47 times higher than the cast ($3.60 \times 10^{-8} \pm 7 \times 10^{-9}$ mm^3/mm) and hot pressed ($1.11 \times 10^{-8} \pm 3 \times 10^{-9}$ mm^3/mm) CoCrMo samples, respectively. Furthermore, wear rate of the cast CoCrMo sample was found three times higher than that of the hot pressed sample.

The microstructure of the cast CoCrMo alloy presents a dentritic structure, while HP CoCrMo alloy presents a granular structure having relatively smaller grain sizes [26]. It has been thought that this difference on the microstructure is also contributed to the difference on the hardness values between the cast and the HP CoCrMo alloy (342 ± 13 HV and 480 ± 25 HV, respectively). Due to the Archard's equation, wear rate is inversely proportional to the hardness of the wearing material [40,53]. Thus, it can be consid-

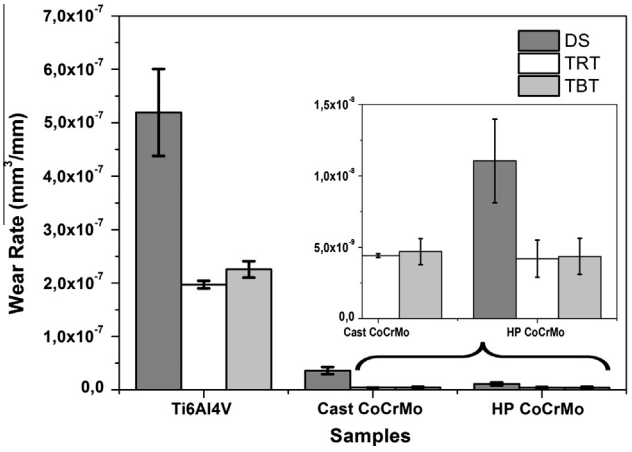

Fig. 11. Wear rate values after dry sliding and tribocorrosion tests (DS: dry sliding, TRT: tribocorrosion at room temperature, and TBT: tribocorrosion at the body temperature).

ered that the microstructure, and therefore the hardness of the CoCrMo alloys had an important influence on the wear resistance.

When wear rates after tribocorrosion tests are considered, it can be seen that in all cases, wear rates are lower than that of the dry sliding tests. It is known that under the tribocorrosion conditions, material loss is usually accelerated due to the synergistic interactions between mechanical action (i.e. sliding) and corrosion [54]. However, it is also well known that under dry sliding conditions, solid particles (i.e. third body particles) may form during the sliding may be entrapped between the sliding surfaces and this situation can seriously affect the friction and wear behaviour [10]. Jiang and Stack studied the sliding wear of Stellite 12 (Co–Cr) alloy against 316 stainless steel under dry and wet (de-ionized water) conditions. The authors reported that under dry sliding conditions, a large amount of wear debris particles were compacted on the 316 stainless steel surface. Those debris protected the steel surface from further wear by forming a protective layer. However, under wet condition, the wear volume of the steel sample was dramatically increased due to the removing of the particles which created the protective layer. On the other hand, the opposite behaviour was observed for the Co–Cr alloy at sliding distances below 1500 m. As a consequence, the wear loss was much higher in dry sliding conditions [54].

Fig. 12 represents the cast CoCrMo sample surfaces after dry sliding and tribocorrosion tests. Even though the samples were cleaned after each test, compacted wear debris are still visible on the dry sliding sample. Therefore, it may be suggested that increased amount of wear rates after dry sliding tests is due to the third body effect. This phenomenon also affected the evolution of the COF graphs, as discussed previously.

In the present study, the tribocorrosion studies were performed both at room and the body temperatures. Because, it is known that the human body temperature of 37 °C may accelerate the electrochemical reactions and therefore corrosion and tribocorrosion damage of the implant materials may be enhanced at the body temperature [55,56]. However, after tribocorrosion studies that were performed at two different temperatures, similar behaviour was observed in terms of worn surface features, evolution of the COF values and electrochemical measurements. Thus, when microstructural and triboelectrochemical data were considered together, it is possible to state that temperature did not affect significantly the tribocorrosion behaviour of the tested samples within the testing conditions.

Another interesting issue related to the wear rate was while wear rate values for CoCrMo samples after tribocorrosion tests were similar, the wear rate of dry sliding cast sample was higher than that of the HP sample. This difference can also be attributed to the third body effect. As explained before, under dry sliding conditions, third body particles were acted as an extra abrasive and it is considered that this behaviour resulted with a higher wear rate for cast CoCrMo alloy in dry sliding conditions. Once that HP CoCrMo alloy has different microstructure (i.e. granular) and higher hardness, the response of the HP sample to this extra abrasive medium was higher than the cast one.

4. Conclusions

Dry sliding and tribocorrosion behaviour of HP CoCrMo alloy was investigated as compared with cast CoCrMo and Ti6Al4V alloys as the most popular commercial biomedical alloys. Within the limitations of this study, the followings can be concluded:

(1) After dry sliding tests, wear mechanism is suggested as mainly a combination of abrasive and adhesive wear for all tested samples.
(2) The temperature did not create any significant difference on the evolution of COF and OCP values during the sliding in NaCl solution. Furthermore, both CoCrMo alloys presented similar behaviour in terms of worn surface features, COF, and OCP. Moreover, when compared to the Ti6Al4V alloy, CoCrMo samples presented lower tendency to corrosion in NaCl solution under sliding.
(3) After dry sliding tests, the wear rate of Ti6Al4V alloy was found 14 and 47 times higher than the cast and HP CoCrMo samples, respectively. Furthermore, wear rate of the cast CoCrMo samples were found three times higher than that of the hot pressed sample. On the other hand, wear rates

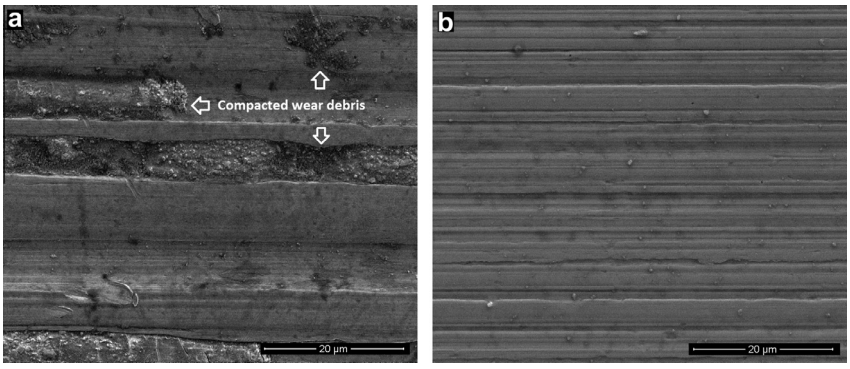

Fig. 12. Cast CoCrMo worn surfaces after (a) dry sliding, and (b) tribocorrosion tests.

after tribocorrosion test presented different values; while wear rates of CoCrMo samples presented similar values, wear rate of Ti6Al4V was found approx. 45 times higher than the both CoCrMo samples. The difference on wear rates between dry sliding and tribocorrosion is mainly attributed to the three-body effect that occurred during the dry sliding wear tests.

(4) Due to those results, it may be suggested that hot pressing can be considered as a simple and low cost alternative production route for CoCrMo implant materials.

In order to avoid the complexity of physiological body fluids, 8 g/l of NaCl was used as an electrolyte as the major compound of Hank's Balanced Salt Solution (HBSS) and Phosphate Buffered Saline (PBS) physiological solutions. However, in order to get more closer to the in vivo conditions, tribocorrosion behaviour of HP CoCrMo alloy should also be studied in physiological solutions, together with the presence of proteins and bio-organisms. On the other hand, the variations of the pH and metal ion content of the electrolyte after the tribocorrosion tests should be considered in order to have a better understanding to the tribocorrosion behaviour. Thus, those issues should be studied in the future work.

Acknowledgements

This study was partially supported by Project SOP HRD – TOP ACADEMIC 76822 and Centre for Mechanical and Materials Technologies (CT2M) in Portugal.

References

[1] Molinari A, Straffelini G, Tesi B, Bacci T. Dry sliding wear mechanisms of the Ti6Al4V alloy. Wear 1997;208:105–12.
[2] Long M, Rack HJ. Titanium alloys in total joint replacement – a materials science perspective. Biomaterials 1998;19:1621–39.
[3] Ganesh BKC, Ramanaih N. Chandrasekhar Rao P V. dry sliding wear behavior of Ti–6Al–4V implant alloy subjected to various surface treatments. Trans Indian Inst Metals 2012;65:425–34.
[4] Dourandish M, Godlinski D, Simchi A, Firouzdor V. Sintering of biocompatible P/M Co–Cr–Mo alloy (F-75) for fabrication of porosity-graded composite structures. Mater Sci Eng: A 2008;472:338–46.
[5] Niinomi M. Recent metallic materials for biomedical applications. Metall Mater Trans A 2002;33:477–86.
[6] Varano R, Bobyn JD, Medley JB, Yue S. Effect of microstructure on the dry sliding friction behavior of CoCrMo alloys used in metal-on-metal hip implants. J Biomed Mater Res. Part B, Appl Biomater 2006;76:281–6.
[7] Thomann UI, Uggowitzer PJ. Wear–corrosion behavior of biocompatible austenitic stainless steels. Wear 2000;239:48–58.
[8] Marino CEB, Mascaro LH. EIS characterization of a Ti-dental implant in artificial saliva media: dissolution process of the oxide barrier. J Electroanal Chem 2004;568:115–20.
[9] Yan Y, Neville A, Dowson D. Biotribocorrosion – an appraisal of the time dependence of wear and corrosion interactions: I. The role of corrosion. J Phys D: Appl Phys 2006;39:3200–5.
[10] Landolt D, Mischler S, Stemp M, Barril S. Third body effects and material fluxes in tribocorrosion systems involving a sliding contact. Wear 2004;256:517–24.
[11] Sargeant A, Goswami T. Hip implants – Paper VI – ion concentrations. Mater Des 2007;28:155–71.
[12] Borgioli F, Galvanetto E, Iozzelli F, Pradelli G. Improvement of wear resistance of Ti–6Al–4V alloy by means of thermal oxidation. Mater Lett 2005;59:2159–62.
[13] Ming Q, Yong-zhen Z, Jian-heng Y, Jun Z. Microstructure and tribological characteristics of Ti–6Al–4V alloy against GCr15 under high speed and dry sliding. Mater Sci Eng: A 2006;434:71–5.
[14] Alam MO, Haseeb ASMA. Response of Ti–6Al–4V and Ti–24Al–11Nb alloys to dry sliding wear against hardened steel. Tribol Int 2002;35:357–62.
[15] Saldívar-García AJ, López HF. Microstructural effects on the wear resistance of wrought and as-cast Co–Cr–Mo–C implant alloys. J Biomed Mater Res Part A 2005;74:269–74.
[16] Hsu H-C, Lian S-S. Wear properties of Co–Cr–Mo–N plasma-melted surgical implant alloys. J Mater Process Technol 2003;138:231–5.
[17] Barril S, Mischler S, Landolt D. Electrochemical effects on the fretting corrosion behaviour of Ti6Al4V in 0.9% sodium chloride solution. Wear 2005;259:282–91.
[18] Chen J, Yan F. Tribocorrosion behaviors of Ti–6Al–4V and Monel K500 alloys sliding against 316 stainless steel in artificial seawater. Trans Nonferr Metals Soc China 2012;22:1356–65.
[19] Martin É, Azzi M, Salishchev GA, Szpunar J. Influence of microstructure and texture on the corrosion and tribocorrosion behavior of Ti–6Al–4V. Tribol Int 2010;43:918–24.
[20] Dimah MK, Devesa Albeza F, Amigó Borrás V, Igual Muñoz A. Study of the biotribocorrosion behaviour of titanium biomedical alloys in simulated body fluids by electrochemical techniques. Wear 2012;294–295:409–18.
[21] Igual Muñoz A, Casabán Julián L. Influence of electrochemical potential on the tribocorrosion behaviour of high carbon CoCrMo biomedical alloy in simulated body fluids by electrochemical impedance spectroscopy. Electrochim Acta 2010;55:5428–39.
[22] Mathew MT, Runa MJ, Laurent M, Jacobs JJ, Rocha LA, Wimmer MA. Tribocorrosion behavior of CoCrMo alloy for hip prosthesis as a function of loads: a comparison between two testing systems. Wear 2011;271:1210–9.
[23] Yan Y, Neville A, Dowson D, Williams S. Tribocorrosion in implants—assessing high carbon and low carbon Co–Cr–Mo alloys by in situ electrochemical measurements. Tribol Int 2006;39:1509–17.
[24] Giacchi JV, Morando CN, Fornaro O, Palacio HA. Microstructural characterization of as-cast biocompatible Co–Cr–Mo alloys. Mater Charact 2011;62:53–61.
[25] Bolzoni L, Ruiz-Navas EM, Neubauer E, Gordo E. Mechanical properties and microstructural evolution of vacuum hot-pressed titanium and Ti–6Al–7Nb alloy. J Mech Beh Biomed Mater 2012;9:91–9.
[26] Henriques B, Soares D, Silva FS. Microstructure, hardness, corrosion resistance and porcelain shear bond strength comparison between cast and hot pressed CoCrMo alloy for metal–ceramic dental restorations. J Mech Beh Biomed Mater 2012;12:83–92.
[27] Bolzoni L, Meléndez IM, Ruiz-Navas EM, Gordo E. Microstructural evolution and mechanical properties of the Ti–6Al–4V alloy produced by vacuum hot-pressing. Mater Sci Eng: A 2012;546:189–97.
[28] Bolzoni L, Ruiz-Navas EM, Neubauer E, Gordo E. Inductive hot-pressing of titanium and titanium alloy powders. Mater Chem Phys 2012;131:672–9.
[29] Mischler S. Triboelectrochemical techniques and interpretation methods in tribocorrosion: a comparative evaluation. Tribol Int 2008;41:573–83.
[30] Zivic F, Babic M, Vencl A. Continuous control as alternative route for wear monitoring by measuring penetration depth during linear reciprocating sliding of Ti6Al4V alloy. J Alloys Compd 2011;509:5748–54.
[31] Dong H, Bell T. Tribological behaviour of alumina sliding against Ti6Al4V in unlubricated contact. Wear 1999;225–229:874–84.
[32] Deuis RL, Subramanian C, Yellup JM. Dry sliding wear of aluminium composites - a review. Compos Sci Technol 1997;57:415–35.
[33] Toptan F, Kerti I, Rocha LA. Reciprocal dry sliding wear behaviour of B4Cp reinforced aluminium alloy matrix composites. Wear 2012;290–291:74–85.
[34] Qu J, Blau PJ, Watkins TR, Cavin OB, Kulkarni NS. Friction and wear of titanium alloys sliding against metal, polymer, and ceramic counterfaces. Wear 2005;258:1348–56.
[35] Straffelini G, Molinari A. Dry sliding wear of Ti–6Al–4V alloy as influenced by the counterface and sliding conditions. Wear 1999;236:328–38.
[36] Mu D, Shen B, Zhao X. Effects of boronizing on mechanical and dry-sliding wear properties of CoCrMo alloy. Mater Des 2010;31:3933–6.
[37] Wimmer M, Loos J, Nassutt R, Heitkemper M, Fischer A. The acting wear mechanisms on metal-on-metal hip joint bearings: in vitro results. Wear 2001;250:129–39.
[38] Kehler B, Baker N, Lee D, Maggiore C, Nastasi M, Tesmer J, et al. Tribological behavior of high-density polyethylene in dry sliding contact with ion-implanted CoCrMo. Surf Coat Technol 1999;114:19–28.
[39] Mcaiieter BAJ. The Al–Co (aluminum–cobalt) system. J Phase Equilibr 1989;10:646–50.
[40] Lashgari HR, Zangeneh S, Ketabchi M. Isothermal aging effect on the microstructure and dry sliding wear behavior of Co–28Cr–5Mo–0.3C alloy. J Mater Sci 2011;46:7262–74.
[41] Manivasagam G, Dhinasekaran D, Rajamanickam A. Biomedical implants : corrosion and its prevention – a review. Recent Pat Corros Sci 2010;2:40–54.
[42] Bettini E, Eriksson T, Boström M, Leygraf C, Pan J. Influence of metal carbides on dissolution behavior of biomedical CoCrMo alloy: SEM, TEM and AFM studies. Electrochim Acta 2011;56:9413–9.
[43] Diomidis N, Göçkan N, Ponthiaux P, Wenger F, Celis J-P. Assessment of the surface state behaviour of Al71Cu10Fe9Cr10 and Al3Mg2 complex metallic alloys in sliding contacts. Intermetallics 2009;17:930–7.
[44] Diomidis N, Mischler S, More NS, Roy M. Tribo-electrochemical characterization of metallic biomaterials for total joint replacement. Acta Biomater 2012;8:852–9.
[45] Zhao W, Liu C, Dong L, Wang Y. Effects of arc spray process parameters on corrosion resistance of Ti coatings. J Therm Spray Technol 2009;18:702–7.
[46] Landolt D, Mischler S, Stemp M. Electrochemical methods in tribocorrosion: a critical appraisal. Electrochim Acta 2001;46:3913–29.
[47] Contu F, Elsener B, Böhni H. A study of the potentials achieved during mechanical abrasion and the repassivation rate of titanium and Ti6Al4V in inorganic buffer solutions and bovine serum. Electrochim Acta 2004;50:33–41.
[48] Hanawa T, Asami K, Asaoka K. Repassivation of titanium and surface oxide film regenerated in simulated bioliquid. J Biomed Mater Res 1998;40:530–8.
[49] Manhabosco TM, Tamborim SM, Dos Santos CB, Müller IL. Tribological, electrochemical and tribo-electrochemical characterization of bare and

nitrided Ti6Al4V in simulated body fluid solution. Corros Sci 2011;53:1786–93.
[50] Buford A, Goswami T. Review of wear mechanisms in hip implants : Paper I – General. Mater Des 2004;25:385–93.
[51] Mcgee MA, Howie DW, Costi K, Haynes DR, Wildenauer CI, Pearcy MJ, et al. Implant retrieval studies of the wear and loosening of prosthetic joints : a review. Wear 2000;241:158–65.
[52] España FA, Balla VK, Bose S, Bandyopadhyay A. Design and fabrication of CoCrMo alloy based novel structures for load bearing implants using laser engineered net shaping. Mater Sci Eng: C 2010;30:50–7.
[53] Zangeneh S, Lashgari HR, Roshani A. Microstructure and tribological characteristics of aged Co–28Cr–5Mo–0.3C alloy. Mater Des 2012;37:292–303.
[54] Jiang J, Stack MM. Modelling sliding wear: from dry to wet environments. Wear 2006;261:954–65.
[55] Figueiredo-Pina CG, Neves AAM, Neves BMB Das. Corrosion-wear evaluation of a UHMWPE/Co–Cr couple in sliding contact under relatively low contact stress in physiological saline solution. Wear 2011;271:665–70.
[56] Pakshir M, Bagheri T, Kazemi MR. In vitro evaluation of the electrochemical behaviour of stainless steel and Ni–Ti orthodontic archwires at different temperatures. Eur J Orthod 2011:1–7.